Development of an Autonomous Modular Swimming Robot with Disturbance Rejection and Path Tracking

Hankun Deng^{1,†}, Colin Nitroy^{1,†}, Kundan Panta¹, Donghao Li¹, Shashank Priya² and Bo Cheng¹, *Member, IEEE*

Abstract— Here we present the development of an autonomous modular swimming robot. This robot, named µBot 2.0, was upgraded from our previous robot platform (µBot) and features onboard computing, sensing, and power. Its compact size and modularity render the robot an ideal platform for studying bio-inspired robot swimming. The robot is equipped with a microcontroller in its head that communicates with external computers through Bluetooth Low Energy (BLE) and sends motor commands to the body segments via Inter-Integrated Circuit (I2C) protocol. Each body segment has a customized printed circuit board (PCB) that receives commands and controls the electromagnetic actuator for generating body movements. The robot head is also equipped with an Inertial Measurement Unit (IMU) to measure its heading and a battery for power. In this work, a µBot 2.0 with three actuators was assembled and the swimming performance was tested. The robot actuators were activated via rhythmic motor input from a central pattern generator (CPG). Experimental results showed that the swimming speed was highly sensitive to the frequency of the motor input, with a maximum swimming speed of 130 mm/s (equivalent to 0.7 body length per second) at 6 Hz. The robot also had the capability to correct its heading with IMU feedback and follow desired paths using a line-of-sight (LOS) guidance law with an overhead camera. Our results demonstrate the effectiveness of the robot's design and its potential in a variety of aquatic applications.

I. INTRODUCTION

Fishes are fascinating swimmers that are capable of fast, agile, and efficient underwater locomotion [1], [2]. They obtained diverse forms in various environments and are able to navigate robustly against disturbance from surrounding flows [3], [4]. For decades, researchers have been studying various aspects of fish locomotion and developing fishinspired underwater vehicles [5]–[7]. Compared with traditional underwater propulsion systems such as propellers and pumps which are usually bulky and generate substantial turbulence [8], bio-inspired propulsion mechanisms are less noisy and easier to scale down, and they have the potential to better accomplish tasks such as underwater exploration, aquatic monitoring and mobile sensing [9], [10].

Research supported by National Science Foundation (CNS-1932130 awarded to B.C), Army Research Office (W911NF-20-1-0226, awarded to B.C), and United States Department of Agriculture (NIFA-2019-67021-28991, awarded to S.P).

²Department of Material Science and Engineering, The Pennsylvania State University, University Park, PA 16802, United States of America.

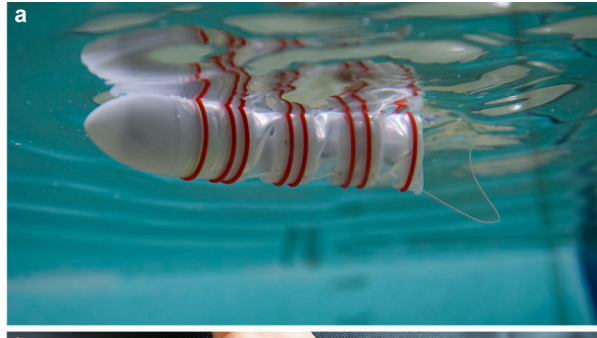




Fig. 1. Photos of an assembled μBot 2.0 with three actuators. (a) A μBot 2.0 is swimming in water. The edge of the caudal fin is highlighted with a gray curve. (b) A μBot 2.0 is held by a hand. Total length of the robot is 19 cm.

On one hand, many fish-inspired robots were developed in tethered lab setup for specific purposes, such as to investigate the propulsion mechanisms of fishes [11]–[13], to obtain optimal morphological design [14]–[16], to verify mathematical models [17], or to test sensing and control strategies [18]–[20].

On the other hand, significant progress has been made in recent years to develop fish-inspired, autonomous robots that are untethered. For example, SoFi is an autonomous undulatory robot that can swim along 3D trajectories [9]. Li et al. developed a ray-like robot that can swim in the Mariana Trench down to a depth of 10,900 meters [21]. Bluebot is a 3D swimmer that is able to replicate the fish's schooling behavior [22]. Zhang et al. built a swimming robot with dual caudal fins [23]. There are also autonomous robots with novel mechanical designs such as wire-driven activation mechanism [24] and double-slider-crank mechanism [25].

Despite these progresses, the state-of-the-art fish-inspired robots remain inferior comparing to fishes in terms of speed, agility and efficiency [11], [24], [26]. In addition, they usually

[†]These authors contributed equally to the paper.

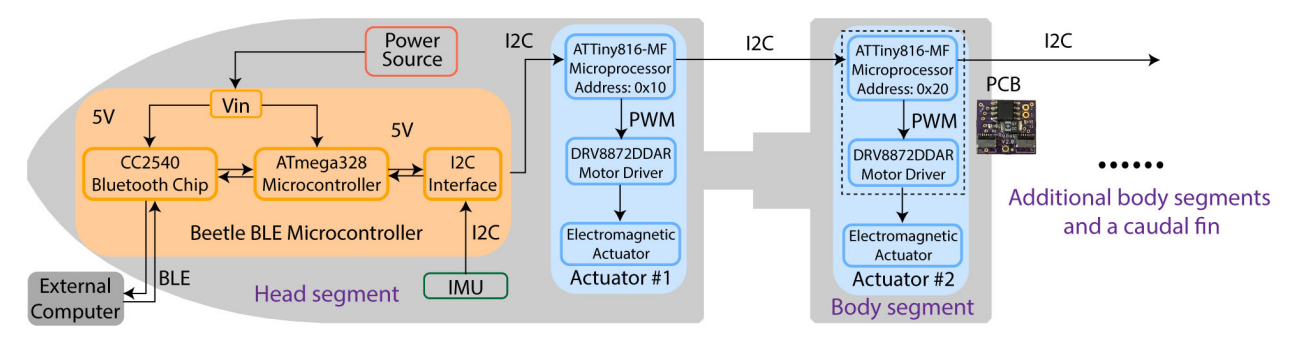


Fig. 2. Communication protocol of μ Bot 2.0. The head segment includes the Beetle BLE microcontroller, the BNO055 IMU, the power source and the first actuator. A body segment contains a PCB (box with dashed line) and an electromagnetic actuator. Body segments are electrically connected with the head segment through ribbon cable. The number of body segments can be easily modified as long as a unique address for each body PCB is provided for I2C communication. The robot can communicate with external computers or smart devices which are BLE compatible. In this work, the sensor readings were collected by a laptop with MATLAB R2020a (MathWorks, Natick, MA, USA).

have relatively large size compared to their biological counterparts, while it is also difficult to alter their body morphology for rapid prototyping. Small, untethered swimming robots are also usually not accessible to high power sources as compared with tethered robots [27], [28].

In our recent work, we developed modular, magnetic, undulatory robots (named $\mu Bot 1.0 [29]$ –[32]) in tethered setting as an experimental platform to explore Fluid-Structure Interaction (FSI) of fish-inspired swimming and to investigate the relationship between the body morphology, the motor inputs, and the swimming performance. In this work, based on the design of $\mu Bot 1.0$, we developed a fully autonomous swimming robot (named $\mu Bot 2.0$, Fig. 1) with onboard battery, computing, and sensing.

In this paper, we present the development of $\mu Bot\ 2.0$ and the experiments to study its swimming performance. Specifically, we first studied the relationship between its swimming speed and motor input frequency. Next, we demonstrated the robot's capability for heading disturbance rejection by using feedback control to bias the motor input. Additionally, a line-of-sight (LOS) guidance law was implemented to showcase the robot's ability for path tracking using an overhead camera. The rest of this paper is organized as follows. In Section II, the electrical design of $\mu Bot\ 2.0$ is presented. Section III introduces mechanical design and assembly. Then the motor program and control algorithms are described in Section IV. Section V presents the experimental results. Finally, conclusions and future work are summarized in Section VI.

II. ELECTRICAL DESIGN

We aimed at upgrading µBot 1.0 so that the robot is able to carry sensors and remotely transmit both sensor and control signals to an external computer. Meanwhile, the power source for all robot functions should be onboard, and the robot should stay operating as long as possible. These requirements led us to use Bluetooth Low Energy (BLE) communication between the robot and external computer and Inter-Integrated Circuit (I2C) communication within the robot, as presented in Fig. 2. BLE, developed for short-range control and monitoring applications, is a low-power wireless technology that requires considerably less energy than Classic Bluetooth [33]. I2C communication enables the robot head (master) to communicate with multiple body segments (slaves).

The core of the μ Bot 2.0 electrical system is the Beetle BLE microcontroller (DFRobot, Shanghai, China), which communicates with the external computer, reads data from sensors, and sends voltage signals to each actuator, behaving as the brain of the robot. This BLE-capable microcontroller is also I2C capable.

Different types of sensors have been equipped in swimming robots, including cameras, pressure sensors, and Inertial Measurement Unit (IMU) [34], [35]. With the information from the sensors, robots are able to achieve various locomotion tasks such as path following or schooling [9], [22]. In this work, a 9-DOF IMU was installed in the head of the μ Bot 2.0. The equipped IMU is BNO055 (Bosch, Gerlingen, Germany), which is also I2C compatible.

Each robot segment houses an identical customized printed circuit board (PCB) and an electromagnetic actuator (Fig. 2). The function of the PCB is to receive the control signals from the Beetle BLE microcontroller and drive the actuator. The circuit board is primarily composed of an 8-bit ATTiny816-MF microprocessor (Microchip, AZ, USA) and a DRV8722DDAR motor driver (Texas Instruments, TX, USA). The microprocessor was programmed to receive two bytes (values between 0-255) from the Beetle BLE and output two PWM signals corresponding to each of those bytes. These PWM signals are sent to the logic inputs of the motor driver, which are used to determine the output voltage sent to the actuator. There are two FFC connectors on the PCB so that each PCB can be connected in series with the master controller and other slave PCBs through flat ribbon cables.

A 7.4V 105mAh lithium-ion battery (series connection of two 3.7V 105mAh batteries, Digi-Key, MN, USA) is used as the power source for the microcontroller, the IMU, and activation of the body actuators. During testing, μBot 2.0 with three actuators can remain on standby for 3.5 hours, or swim continuously for about 20 minutes without switching the battery.

III. MECHANICAL DESIGN

The anatomy of the swimming robot is composed of a larger head segment connected to several identical body segments and lastly, a caudal fin. Actuators are located within the head and body segments, as shown in Fig. 3a. The modular nature of the robot's design allows for a varying number of segments to be utilized for swimming. It has been shown that the majority of steady swimming kinematics of fishes can be

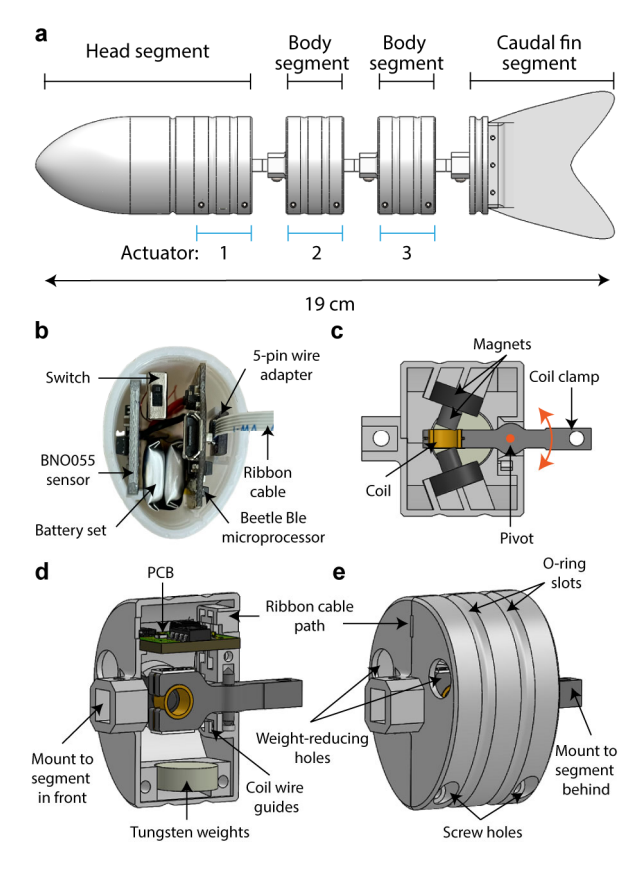


Fig. 3. Mechanical design of μ Bot 2.0. (a) Model of the robot with outer suit removed. (b) Head segment of μ Bot 2.0. (c) Cross-section from the top view of a body segment. (d) Model of a body segment showing inner structure. (e) Model of a body segment without outer suit

described using a series of interconnected multi-segment models with fewer than five segments [36]. Therefore, we built the robot with two body segments so that the whole robot has four segments (Fig. 3a).

A. Head segment mechanical design

The design of the robot's head segment is shown in detail in Fig. 3b (The actuator inside the head segment is not shown). This segment houses a Beetle BLE microcontroller, an IMU, a custom five wire-to-ribbon cable adapter, a battery set, and a power switch. The battery set is placed at the lowest point in the head to ensure a low center of gravity. 32 American Wire Gauge (AWG) magnetic wires connects the electrical components inside the robot head. The 5-pin wire adaptor with ribbon cable connector connects the magnetic wires with the ribbon cable which connects the PCBs in body segments.

B. Body segments design

μBot 2.0 uses electromagnetic actuators that share the same working principle with our previous work [29]. The schematics are presented in Fig.3c. As sent from the motor driver on the PCB, an electric signal is driven through the coil and creates an electromagnetic field, which generates a force pointing to one of the magnets. Inverting the electric signal changes the direction of the electromagnetic field and generates force in the opposite direction. Therefore, the oscillatory motion of the coil and the coil clamp around the

pivot is achieved by generating oscillatory motor input. The range of the rotation angle is $\pm 20^{\circ}$.

The robot's body segments are shown in detail in Fig. 3d and Fig. 3e. The body skeleton is designed to house the PCB and the actuator. The PCB is light (1g) and is placed at the upside of the segment, while a 5g tungsten weight is placed at the bottom side. Two holes are added at the upside to reduce the weight. This design lowers the center of gravity of the segment. The transverse plane of the segment is nearly an ellipse, while the upside is wider than the bottom side, which moves the center of geometry slightly to the upside. Therefore, the center of gravity is set below the center of geometry to achieve roll stability.

The skeleton of a body segment is composed of two pieces fixed together with screws. The screw holes are placed at the bottom side. The ribbon cable path is reserved for electrical connections between the segments. The coil clamp of each segment is mechanically connected to the square mount of the next segment using easily removable screws to enable fast assembly and further increase the modularity of the design. Two O-ring grooves are reserved for O-ring placement during assembly (Fig. 3e).

C. Caudal fin segment design

The caudal fin of μ Bot 2.0 is inspired by pikes. It is made of 0.25 mm thick clear polyvinyl chloride sheet. This thin caudal fin is secured to the 3D printed segment using thin wire threaded through matching holes. This design allows for quick manufacturing of caudal fins with different shapes and stiffness, and caudal fin replacement can be achieved easily.

D. Robot assembly

The robot's structural components were 3D printed in Rigid 4000 photopolymer resin with a Form 2 printer (Formlabs, MA, USA). After assembly, the robot's exterior was covered by a waterproof suit made of silicone rubber (Ecoflex 00-20, Smooth-On Inc, PA, USA). To secure the suit and prevent fluids from entering the robot's electronic control system, silicone O-rings were used, which wrap around the segments and sit in grooves on the body's exterior (Fig. 1).

The average density of μBot 2.0 is slightly less than water so that buoyancy equilibrium is achieved with a minor part of the body (around 5% in depth) above the water surface, therefore achieving 2D swimming. The assembled μBot 2.0 is 19 cm in length, 2.4 cm in width, and 3.2 cm in depth. The overall weight is 85g.

IV. MOTOR PROGRAM AND CONTROL ALGORITHMS

A. Motor program

The majority of the fishes use body and/or caudal fin (BCF) to generate thrust for forward swimming, and these fishes are grouped as BCF swimmers [2] . μ Bot 2.0 also belongs to the BCF form, and swimming robots mimicking BCF swimmers are usually activated with rhythmic motor inputs which can be generated by a central pattern generator (CPG) [37], [38]. The CPG of μ Bot 2.0 is a dual-neuron model proposed by Matsuoka [39]. The overall CPG network is presented in Fig. 4, and each actuator is controlled by a CPG module, including two neurons inhibiting each other. The mathematical expression of each neuron contains two ordinary differential equations (ODEs) as follows,

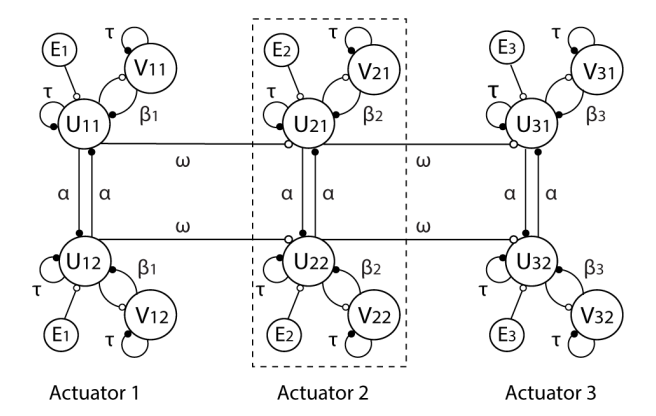


Fig. 4. CPG network of μBot 2.0 with parameters labeled. Dashed box represents a CPG module which includes two neurons inhibiting each other. The voltage applied to the actuators is determined by the output of the CPG modules.

$$\begin{split} \tau \dot{U}_{i,j} + U_{i,j} &= E_i - \beta_i V_{i,j} - \alpha y_{i,3-j} + \omega y_{i-1,j} \\ \tau \dot{V}_{i,j} + V_{i,j} &= y_{i,j} \\ y_{i,j} &= \max \bigl(0, U_{i,j} \bigr) \\ y_{i,out} &= y_{i,1} - y_{i,2} \\ i &= 1, 2, \dots, n; j = 1, 2 \end{split} \tag{1}$$

where U and V are states of the ODEs; n is the CPG module number, which equals the number of actuators; τ is the time constant, which mainly determines the frequency of the rhythmic output; E represents external stimulus for each neuron, controlling the output's intensity; β and α are adaption coefficient and mutual inhibition weight in one module; ω is the inter-module connection weight of the neuron; $y_{i,out}$ is the output of the i^{th} CPG module.

In our previous work, the parameters of the CPG were learned experimentally with a reinforcement learning algorithm [29], and the experimental results showed that swimming speed is highly sensitive to the undulating frequency. In this work, the motor input frequency of μBot 2.0 was varied to show its influence on the swimming speed, which was achieved by modifying the time constant τ . All the other CPG parameters were fixed and listed in TABLE I. The CPG output was scaled by the voltage limit of the onboard battery set.

The overall control diagram is presented in Fig. 5. With motor input from the CPG, the robot undulates its body and interacts with fluid around it. Diverse swimming gaits are generated from the FSI and lead to different swimming

TABLE I. CPG P.	ARAMETERS

Parameter	Values or comments
τ	Varied to change frequency of
ι	the CPG output
$\boldsymbol{E_1}$	62
$\vec{E_2}$	38
E_2 E_3	38
β_1	4.5
β_2	3.5
β_3	3.5
α	3
ω	1

performances. Note that this process is feedforward control. Even though symmetric motor input is applied on the robot for straight swimming, small disturbance from the environment or asymmetricity within the robot might cause the robot to change the heading direction.

B. Feedback control for heading disturbance rejection

With an onboard IMU detecting the heading angle, we can reject the heading disturbance of the robot. A commonly used method to control the robot heading is to add an amplitude offset to the symmetrically rhythmic motor input, which creates an asymmetrical undulation of the body and the caudal fin [40], [41]. The turning rate can be controlled by the magnitude of the offset. Therefore, in the feedback control, the angle error is defined as the difference between the measured robot heading and the reference, and the relationship between the offset and the angle error is:

$$V_{offset} = \frac{7.4 \times 2}{255} \times K_p \times e_{angle} , \qquad (2)$$

where e_{angle} is the angle error (Fig. 5). V_{offset} is the offset voltage, and K_p is the proportional gain. $7.4 \times 2/255$ is a scaling term that maps one-byte data to voltage. This setting makes the robot heading tuning a P control. Then the offset is added to modify the voltage profile:

$$V_{biased} = V_{original} + V_{offset} , (3)$$

where $V_{original}$ is the original voltage profile from the CPG, and V_{biased} is the biased motor input that runs the robot. Fig. 6 shows an example of the motor input from the CPG and the biased motor input. Since the battery can only supply 7.4V voltage, the biased motor input is truncated at the limit voltage.

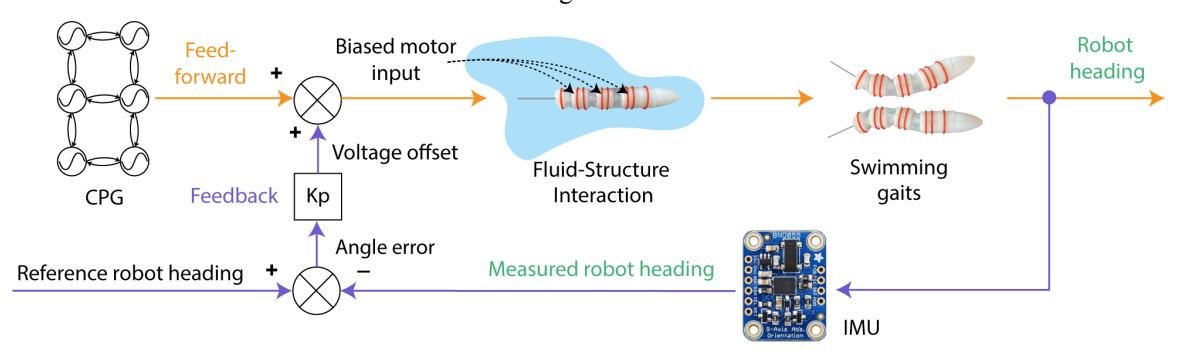


Fig. 5. Overall control diagram for heading disturbance rejection of μBot 2.0, including feedforward and feedback control. The swimming gaits and performance (include robot heading) are generated from the FSI which is modulated by the motor input.

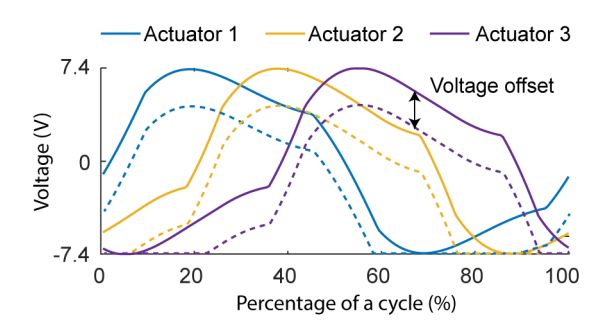


Fig. 6. Example motor input for forward swimming (solid lines) and biased motor input with -3V offset (dashed lines).

C. Line-of-sight (LOS) guidance law for path tracking

Path tracking is an important capability for fish-like robots to navigate through complex environments. In this study, we implemented a line-of-sight (LOS) method, which has been used in snake-like swimming robots [42], to guide the robot along a 2D path, as illustrated in Fig. 7. The basic LOS guidance law specifies the required reference heading for tracking a straight-line path based on the robot's position relative to the path:

$$\theta_{ref} = \arctan(p_v/\Delta),$$
 (4)

where θ_{ref} is the reference heading, p_y is the perpendicular distance from the straight-line path, and Δ , the look-ahead distance, is a tunable parameter that determines how directly the reference heading points towards the path. LOS guidance could thus be used naturally with the controller in (2) by dynamically updating the reference heading for e_{angle} .

The LOS law was extended to follow an arbitrary curved path by dividing the path into multiple straight-line sections between waypoints [43], [44]. The robot switches from tracking one straight line to the next when it enters the "acceptance region" of the next waypoint (Fig. 7). The acceptance region of the i^{th} waypoint, WP_i , is composed of a circular area around WP_i and all the area past WP_i in the direction pointing from WP_{i-1} to WP_i . The distance between waypoints along the reference path, d_{wp} , and the radius of the acceptance region, r_{wp} , are tunable parameters.

During the path tracking experiments, an overhead monochrome camera (acA2000-165umNIR, Basler AG Inc, Ahrensburg, Germany) was used to capture images of the robot swimming [29]. The images were subsequently processed in MATLAB to determine the robot's geometric center, calculate the reference heading, and send the information to the robot in real-time at 50 Hz via BLE communication.

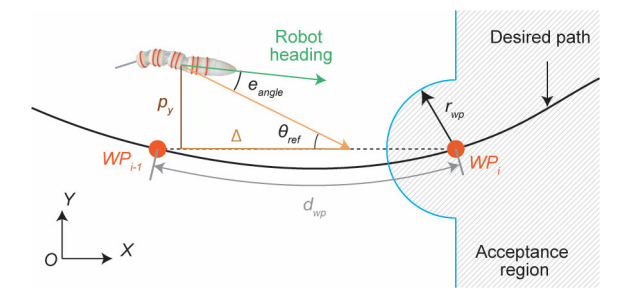


Fig. 7. Illustration of the LOS method with waypoints guidance strategy.

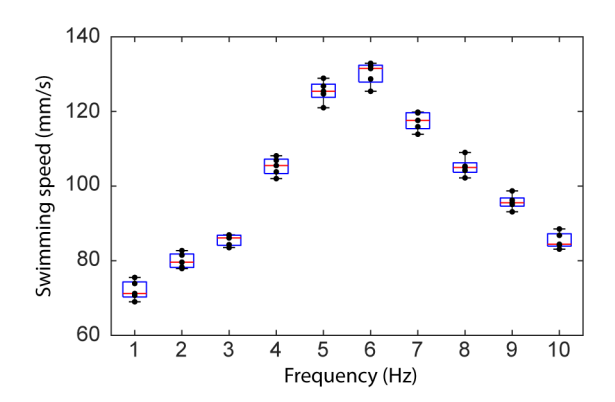


Fig. 8. Relationship between the swimming speed and the frequency of the motor input. Boxplots indicate the distribution of the 5 experiments. Black dots represent the experimental data.

V. EXPERIMENTS

A. Frequency response

The first experiment was to explore the relationship between the frequency of the motor input and the swimming speed. CPG time constant τ in (1) was varied so that the frequency of the motor input changed from 1 Hz to 10 Hz with a 1 Hz increment. The swimming speed was calculated as the distance traveled in one second after the μ Bot reached the steady swimming state. In each test, experiments were repeated 5 times.

The results showed that the swimming speed was highly related to the motor input frequency (Fig. 8), which was in agreement with biological fishes [45] and other swimming robots [17], [46]. The maximum speed (130 mm/s, or 0.7 BL/s) was reached at 6 Hz, which is comparable with other autonomous robots [9], [47].

B. Heading disturbance rejection

The second experiment was to test the capability of μ Bot 2.0 to reject heading disturbance with feedback control. Proportional gain K_p in (2) was empirically selected as 4.5, 1.5, and 0.8. During forward swimming, disturbance was applied to the head of the robot by an experimenter, which pushed the robot laterally and altered its heading, as shown in the supplementary video. The sensor reading and offset voltage are presented in Fig. 9, where the offset voltage was calculated according to the control law (2).

It is clearly illustrated in Fig.9 and the supplementary video that the robot recovered from the disturbance and regained a heading along the reference direction for all the cases. Notably, larger feedback gain K_p did not appear to improve the recovery speed, possibly due to the nonlinearities in the FSI and robot responses, the understanding of which required future work. In general, the recovery time varied among different K_p and between the two disturbances with the same K_p . For example, with $K_p = 4.5$, when pushed to the left side, it took around 2 seconds for μ Bot to recover. But it took almost 4 seconds for the μ Bot to recover when it was pushed to the right side (Fig. 9a). This might be due to the asymmetry of the added disturbance or robot assembly. The timing (percentage of a cycle during robot undulation) when the disturbance is added might also affect the recovery time.

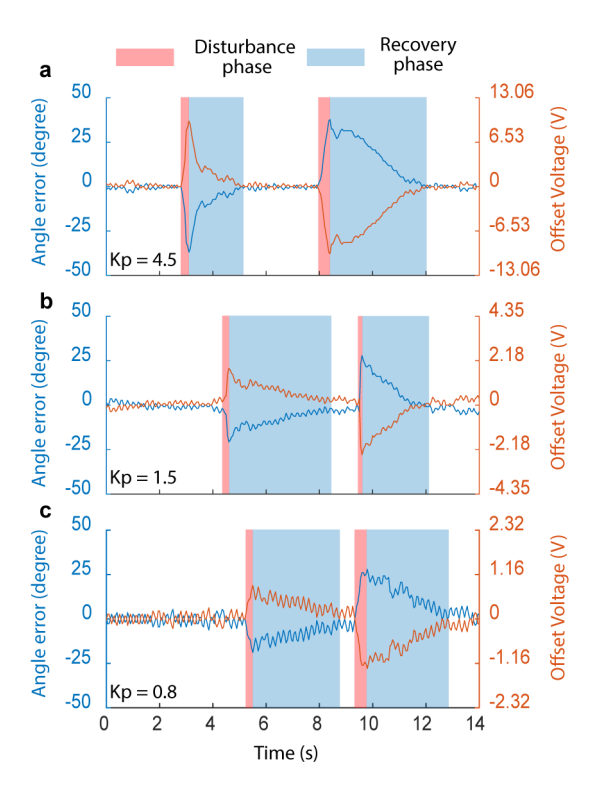


Fig. 9. Sensor readings and offset voltages relative to time in heading disturbance rejection experiments. (a-c) K_p is 4.5, 1.5, and 0.8, respectively. Note that the scaling of the offset voltage is different among the three subplots.

It was also noticed that there were small, high-frequency fluctuations in the sensor reading due to the recoil of the head (Fig. 9). The fluctuations became smaller when K_p increased, indicating that larger K_p reduced head recoil.

C. Path tracking

The third experiment aimed to assess the path tracking capability of the μ Bot 2.0. Two types of reference trajectories were tested, a step function and a sine wave. The LOS law parameters were set empirically as $\Delta=150$ mm, $d_{wp}=100$ mm, and $r_{wp}=150$ mm, while $K_p=4.5$ was used. The obtained results were shown in Fig. 10 and the supplementary video. While the robot was able to track both trajectories with good repeatability, it was unable to execute a 90-degree sharp turn when following the step function due to its limited steering capability. To improve the tracking performance, the robot actuators' rotation angle range needs to be increased. It is also necessary to further refine the control algorithms, such

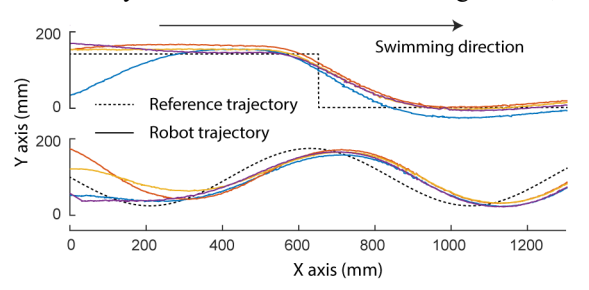


Fig. 10. Results for path tracking experiments. Dashed line is the reference trajectory, and the solid lines are the robot trajectories from the overhead camera.

as systematic design of the LOS parameters and optimization of the motor control for robot turning.

VI. CONCLUSIONS AND FUTURE WORK

In this study, we introduced µBot 2.0, an autonomous swimming robot featuring modular body segments and compact size. The robot, which contained a microcontroller in the head and a customized PCB in each body segment, was able to communicate with external computers, read sensor data, and control body segments. During experiments, the robot's swimming speed was found to be highly sensitive to the motor input frequency, and the maximum swimming speed of the robot was measured to be 130 mm/s (0.7 BL/s) at 6 Hz. Additionally, the robot was able to reject heading disturbance using feedback control, and it demonstrated good repeatability while tracking two reference trajectories, a step function, and a sine wave. The features of µBot 2.0 make it a good platform for studying fish-inspired swimming, and it has potential to achieve tasks such as underwater exploration, aquatic monitoring, and mobile sensing.

The results of the heading disturbance rejection experiment showed that the recovery time was not improved with a larger proportional gain K_p . It is worth noting that the magnitude and timing of the disturbance may also have affected the recovery time. In future work, the factors that affect the recovery time will be further investigated, and the combined CPG motor program and feedback control will be optimized to minimize the time. Additionally, the limit of the robot's maneuverability will be explored, and control strategies will be optimized to improve the robot's tracking capability. These efforts will advance our understanding of fish-like robots' swimming performance and contribute to the development of more efficient and agile underwater vehicles.

Note that $\mu Bot\ 2.0$ can only achieve 2D swimming below the water surface. To enable 3D swimming, a buoyancy control mechanism is needed. We are currently adding pectoral fins for upwards/downwards force generation. To achieve a miniature size, a bio-inspired shape memory alloy composite (BISMAC) actuator will be used for the fins [48].

REFERENCES

- [1] P. Domenici and R. W. Blake, "The kinematics and performance of fish fast-start swimming," *Journal of Experimental Biology*, vol. 200, no. 8, pp. 1165–1178, 1997.
- [2] M. Sfakiotakis, D. M. Lane, and J. B. C. Davies, "Review of fish swimming modes for aquatic locomotion," *IEEE Journal of Oceanic Engineering*, vol. 24, no. 2, pp. 237–252, 1999.
- [3] M. Gazzola, M. Argentina, and L. Mahadevan, "Scaling macroscopic aquatic locomotion," *Nature Physics*, vol. 10, no. 10, pp. 758–761, 2014.
- [4] J. C. Liao, "A review of fish swimming mechanics and behaviour in altered flows," *Philosophical Transactions of the Royal Society* B: Biological Sciences, vol. 362, no. 1487, pp. 1973–1993, 2007.
- [5] N. Kamamichi, M. Yamakita, K. Asaka, and Z. W. Luo, "A snake-like swimming robot using IPMC actuator/sensor," in *Proceedings of the 2006 IEEE International Conference on Robotics and Automation*, 2006, pp. 1812–1817.
- [6] F. Xie, Z. Li, Y. Ding, Y. Zhong, and R. Du, "An Experimental Study on the Fish Body Flapping Patterns by Using a Biomimetic Robot Fish," *IEEE Robotics and Automation Letters*, vol. 5, no. 1, pp. 64–71, 2020.
- [7] J. Shintake, D. Zappetti, T. Peter, Y. Ikemoto, and D. Floreano, "Bio-inspired Tensegrity Fish Robot," in 2020 IEEE International Conference on Robotics and Automation (ICRA), 2020, pp. 2887– 2892.

- [8] H. Deng, "Analysis and design of an in-line pump as a thruster for swimming robots," Rice University, 2018.
- [9] R. K. Katzschmann, J. DelPreto, R. MacCurdy, and D. Rus, "Exploration of underwater life with an acoustically controlled soft robotic fish," *Science Robotics*, vol. 3, no. 16, p. eaar3449, 2018.
- [10] J. Yu, C. Zhang, and L. Liu, "Design and control of a single-motor-actuated robotic fish capable of fast swimming and maneuverability," *IEEE/ASME Transactions on Mechatronics*, vol. 21, no. 3, pp. 1711–1719, 2016.
- [11] J. Zhu, C. White, D. K. Wainwright, V. Di Santo, G. V. Lauder, and H. Bart-Smith, "Tuna robotics: A high-frequency experimental platform exploring the performance space of swimming fishes," Science Robotics, vol. 4, no. 34, p. eaax4615, 2019.
- [12] C. H. White, G. V Lauder, and H. Bart-Smith, "Tunabot Flex: a tuna-inspired robot with body flexibility improves highperformance swimming," *Bioinspiration & Biomimetics*, vol. 16, no. 2, p. 026019, 2021.
- [13] L. Wen, T. Wang, G. Wu, and J. Liang, "Quantitative thrust efficiency of a self-propulsive robotic fish: Experimental method and hydrodynamic investigation," *IEEE/ASME Transactions on Mechatronics*, vol. 18, no. 3, pp. 1027–1038, 2013.
- [14] Y. Shan, Y. Bayiz, and B. Cheng, "Efficient Thrust Generation in Robotic Fish Caudal Fins using Policy Search," *IET Cyber-Systems and Robotics*, vol. 1, no. 1, pp. 38–44, 2019.
- [15] K. L. Feilich and G. V Lauder, "Passive mechanical models of fish caudal fins: Effects of shape and stiffness on self-propulsion," *Bioinspiration & Biomimetics*, vol. 10, no. 3, p. 036002, 2015.
- [16] K. H. Low and C. W. Chong, "Parametric study of the swimming performance of a fish robot propelled by a flexible caudal fin," *Bioinspiration & Biomimetics*, vol. 5, no. 4, 2010.
- [17] Q. Zhong et al., "Tunable stiffness enables fast and efficient swimming in fish-like robots," Science Robotics, vol. 6, p. eabe4088, 2021.
- [18] C. J. Esposito, J. L. Tangorra, B. E. Flammang, and G. V Lauder, "A robotic fish caudal fin: Effects of stiffness and motor program on locomotor performance," *Journal of Experimental Biology*, vol. 215, no. 1, pp. 56–67, 2012.
- [19] R. J. Clapham and H. Hu, "ISplash-I: High performance swimming motion of a carangiform robotic fish with full-body coordination," in 2014 IEEE International Conference on Robotics and Automation (ICRA), 2014, pp. 322–327.
- [20] B. Pollard and P. Tallapragada, "Learning hydrodynamic signatures through proprioceptive sensing by bioinspired swimmers," *Bioinspiration & Biomimetics*, vol. 16, no. 2, p. 026014, 2021.
- [21] G. Li et al., "Self-powered soft robot in the Mariana Trench," Nature, vol. 591, no. 7848, pp. 66–71, 2021.
- [22] F. Berlinger, M. Gauci, and R. Nagpal, "Implicit coordination for 3D underwater collective behaviors in a fish-inspired robot swarm," *Science Robotics*, vol. 6, no. 50, 2021.
- [23] S. Zhang, Y. Qian, P. Liao, F. Qin, and J. Yang, "Design and Control of an Agile Robotic Fish with Integrative Biomimetic Mechanisms," *IEEE/ASME Transactions on Mechatronics*, vol. 21, no. 4, pp. 1846–1857, 2016.
- [24] Y. Zhong, Z. Li, and R. Du, "A Novel Robot Fish with Wire-Driven Active Body and Compliant Tail," *IEEE/ASME Transactions on Mechatronics*, vol. 22, no. 4, pp. 1633–1643, 2017.
- [25] W. Zuo, F. Fish, and Z. Chen, "Bio-Inspired Design, Modeling, and Control of Robotic Fish Propelled by a Double-Slider-Crank Mechanism Driven Tail," *Journal of Dynamic Systems, Measurement and Control, Transactions of the ASME*, vol. 143, no. 12, pp. 1–10, 2021.
- [26] K. Struebig, B. Bayat, P. Eckert, A. Looijestijn, T. C. Lueth, and A. J. Ijspeert, "Design and development of the efficient anguilliform swimming robot-MAR," *Bioinspiration & Biomimetics*, vol. 15, no. 3, 2020.
- [27] F. Berlinger, M. Duduta, H. Gloria, D. Clarke, R. Nagpal, and R. Wood, "A Modular Dielectric Elastomer Actuator to Drive Miniature Autonomous Underwater Vehicles," in 2018 IEEE International Conference on Robotics and Automation (ICRA), 2018, pp. 3429–3435.
- [28] F. Berlinger, M. Saadat, H. Haj-Hariri, G. V. Lauder, and R. Nagpal, "Fish-like three-dimensional swimming with an autonomous, multi-fin, and biomimetic robot," *Bioinspiration & Machine Methodology*

- Biomimetics, vol. 16, no. 2, p. 026018, 2021.
- [29] H. Deng, P. Burke, D. Li, and B. Cheng, "Design and experimental learning of swimming gaits for a magnetic, modular, undulatory robot," in 2021 IEEE/RSJ International Conference on Intelligent Robots and Systems (IROS), 2021, pp. 9562–9568.
- [30] D. Li, H. Deng, Y. E. Bayiz, and B. Cheng, "Effects of Design and Hydrodynamic Parameters on Optimized Swimming for Simulated, Fish-inspired Robots," in 2022 IEEE International Conference on Intelligent Robots and Systems (IROS), 2022, pp. 7500–7506.
- [31] H. Deng, D. Li, K. Panta, and B. Cheng, "Magnetic, modular, undulatory robots as robophysical models for exploration of fishinspired swimming," *Bulletin of the American Physical Society*, 2023.
- [32] H. Deng, D. Li, C. Nitroy, A. Wertz, S. Priya, and B. Cheng, "Robot motor learning shows emergence of frequency-modulated, robust swimming with an invariant Strouhal number," arXiv preprint arXiv:2307.08178, 2023.
- [33] C. Gomez, J. Oller, and J. Paradells, "Overview and evaluation of bluetooth low energy: An emerging low-power wireless technology," *Sensors (Switzerland)*, vol. 12, no. 9, pp. 11734–11753, 2012.
- [34] W. Wang and G. Xie, "CPG-based locomotion controller design for a boxfish-like robot," *International Journal of Advanced Robotic Systems*, vol. 11, no. 1, 2014.
- [35] T. Salumäe, I. Rañó, O. Akanyeti, and M. Kruusmaa, "Against the flow: A Braitenberg controller for a fish robot," in 2012 IEEE International Conference on Robotics and Automation, 2012, pp. 4210–4215.
- [36] O. Akanyeti et al., "Fish-inspired segment models for undulatory steady swimming," Bioinspiration and Biomimetics, vol. 17, no. 4, 2022.
- [37] X. Wu and S. Ma, "CPG-based control of serpentine locomotion of a snake-like robot," *Mechatronics*, vol. 20, no. 2, pp. 326–334, 2010.
- [38] A. J. Ijspeert, A. Crespi, D. Ryczko, and J. M. Cabelguen, "From swimming to walking with a salamander robot driven by a spinal cord model," *Science*, vol. 315, no. 5817, pp. 1416–1420, 2007.
- [39] K. Matsuoka, "Sustained oscillations generated by mutually inhibiting neurons with adaptation," *Biological Cybernetics*, vol. 52, no. 6, pp. 367–376, 1985.
- [40] K. Hirata, T. Takimoto, and K. Tamura, "Study on Turning Performance of a Fish Robot," *First International Symposium on Aqua Bio-Mechanisms*, pp. 287–292, 2000.
- [41] S. P. Howe, A. R. Duff, and H. C. Astley, "Comparing the turn performance of different motor control schemes in multilink fishinspired robots," *Bioinspiration & Biomimetics*, vol. 16, no. 3, 2021.
- [42] E. Kelasidi, P. Liljebäck, K. Y. Pettersen, and J. T. Gravdahl, "Innovation in underwater robots: biologically inspired swimming snake robots," *IEEE Robotics & Automation Magazine*, vol. 23, no. 1, pp. 44–62, 2016.
- [43] E. Kelasidi, K. Y. Pettersen, and J. T. Gravdahl, "A waypoint guidance strategy for underwater snake robots," in 2014 22nd Mediterranean Conference on Control and Automation, MED 2014, 2014, pp. 1512–1519.
- [44] P. Liljebäck and K. Y. Pettersen, "Waypoint guidance control of snake robots," in 2011 IEEE International Conference on Robotics and Automation, 2011, pp. 937–944.
- [45] K. Nashimoto, "The Swimming Speed of Fish in Relation to Fish Size and Frequency of Tail Beating," *Nippon Suisan Gakkaishi*, vol. 46, no. 3, pp. 307–312, 1980.
- [46] Y. J. Park, U. Jeong, J. Lee, S. R. Kwon, H. Y. Kim, and K. J. Cho, "Kinematic condition for maximizing the thrust of a Robotic Fish using a compliant caudal fin," *IEEE Transactions on Robotics*, vol. 28, no. 6, pp. 1216–1227, 2012.
- [47] J. Yu, Z. Wu, M. Wang, and M. Tan, "CPG Network Optimization for a Biomimetic Robotic Fish via PSO," *IEEE Transactions on Neural Networks and Learning Systems*, vol. 27, no. 9, pp. 1962–1968, 2016.
- [48] A. A. Villanueva, K. B. Joshi, J. B. Blottman, and S. Priya, "A bioinspired shape memory alloy composite (BISMAC) actuator," *Smart Materials and Structures*, vol. 19, no. 2, 2010.